HEFAT2014
10th International Conference on Heat Transfer, Fluid Mechanics and Thermodynamics
14 – 16 July 2014
Orlando, Florida

A FAST NUMERICAL MODEL TO CALCULATE THE THERMAL PERFORMANCE OF A HEAT EXCHANGER WITH RECTANGULAR PCM STORAGE

Prieto MM.† *, Suárez I.* and González B.**
† Author for correspondence, e-mail: manuelap@uniovi.es
*Energy Department, University of Oviedo, Campus de Viesques s/n, 33204 Gijón (Asturias) SPAIN – Group associated to the Spanish Scientific Research Council (CSIC)
**Energy Department, University of Oviedo, Campus de Viesques s/n, 33204 Gijón (Asturias) SPAIN

ABSTRACT

The use of phase change materials (PCM) in heat exchangers for energy storage and release is under research. CFD modelling is extremely expensive regarding computational resources and time. For example, a PCM heat exchanger that would be used in a domestic heating system could reach a size of 0.8×0.6×0.6 m^3, which is a lot to apply CFD commercial software. Nowadays, there is also a lack of knowledge about the thermal performance of these systems during the loading and unloading processes. Besides, many phase change substances can be used. This work presents an analysis of the thermal performance of a paraffin that would be used in a PCM heat exchanger of a heating system, being the operating temperatures of the heating fluid around 80 ºC at the supply and 30 ºC at the return.

A fast model has been developed. This model takes into account the results of a CFD commercial model, but the knowledge of this model was summarized into useful polynomial equations. These equations, coupled with finite volume equations for the aluminium covering of the PCM and for the heating fluid, were implemented in a Matlab R2012a program and applied to a module consisting of two parallel flat plates separated by 30 mm thickness of PCM, which would be used in a heat exchanger. Two different spatial positions of the module, horizontal and vertical, and two phase change processes, melting and solidification, were studied. The horizontal position is faster than the vertical one, the melting time being nearly twice with respect to the vertical position.

The results of the fast model were compared satisfactorily with the results of a full CFD model solved in Ansys Fluent 14.5. For the same boundary conditions in both models, the computational time diminishes from several weeks to few days.

INTRODUCTION

Thermal energy storage in phase change materials (PCM) is one of the most promising alternatives to improve energy efficiency and reduce primary energy consumption in buildings. These systems allow mitigating the imbalance between demand and consumption of energy by reducing the load peaks and recovering residual heat from air conditioning systems (use of microgeneration systems, thermal solar collectors, etc.) [1,2]. One of the objectives of the study of PCM in air conditioning systems is to find out which is the most suitable phase change substance, considering its storage capability, the capacity of absorbing and releasing heat (melting and solidification velocity) and the price. Regarding the heat transfer characterization of most of the PCM suitable for operating in specific heat exchangers used in thermal systems of buildings, there are no enough data in the open literature to deal conveniently with the design of these heat exchangers, although several references appear in the open literature. In [3] a quite complete volume difference method for a multitubular heat exchanger is presented. Most of the methods apply the enthalpy method to foretell distributions of temperature [4-7] and the majority of the papers deal with the effective-NTU approach [7,8].

In order to solve this lack of data, CFD numerical methods available in commercial software (from now on they are just called CFD) may be used, but they are extremely expensive regarding computational resources and time, so a complete study of the PCM heat exchanger required for the heating system of a 100 m^2 household, approximately 0.8×0.6×0.6 m^3 referring to its size, is practically unreachable. Subsequently, the development of faster numerical models than those based on commercial CFD software is needed to study future PCM heat exchangers along with the building and its thermal systems.

This work presents a CFD analysis of the thermal performance during the solidification-melting phase change of the paraffin RT60 [9], that would be used in a PCM heat exchanger of a heating system, being the operating temperatures of the heating/cooling fluid between 80 ºC and 30 ºC. The CFD model is solved using the software Ansys Fluent 14.5 [10] in a rectangular PCM domain of 30 mm thickness of paraffin and considering two different spatial positions:

horizontal and vertical. Boundary conditions of the first kind (constant temperature) are applied to the boundary surfaces.

The CFD model calculates the evolution along time of the heat flux and the volumetric fraction of the paraffin liquid phase for the defined values of the paraffin and temperature at surfaces of its boundaries, and for both spatial positions of the rectangular PCM. These results are adjusted by mathematical functions that allow the interpolation of the heat flux and volumetric fraction of the liquid for any value of the parameters within their variation ranges.

Then, the mathematical functions obtained from the CFD model are implemented in a fast numerical model, based on the finite volume method, which considers the heat transfer in the PCM module (paraffin and aluminium covering) and in the fluid of the heating system in a coupled way that means boundary conditions of the third kind.

Finally, the results of the fast numerical model applied to a rectangular PCM module heated/cooled by water are compared to the results obtained from the full CFD model, coupling the domains of the aluminium covering and the heating/cooling fluid in chosen essays, which purpose is the comparison of the models.

NOMENCLATURE

A	[m^2]	Area of the cell surfaces
A_{mush}	[kg/s m^3]	Constant in equation (2)
c_p	[J/kg K]	Specific heat at constant pressure
e_{ch}	[m]	Thickness of the cooling/heating fluid channel
e_{PCM}	[m]	Thickness of the PCM
h	[W/m^{2}K]	Convection heat transfer coefficient
i	[J/kg]	Specific enthalpy
k	[W/m K]	Thermal conductivity
L	[m]	Length of the PCM module
L_c	[m]	Characteristic length
$\dot{m}_{ch}$	[kg/s]	Mass flow rate of the cooling/heating fluid in the channel
Nu	[-]	Nusselt number
Pr	[-]	Prandtl number
$\dot{q}_{w,1}$	[W/m^2]	Heat flux through the aluminium wall in contact with the PCM
$\dot{q}_{w,2}$	[W/m^2]	Heat flux through the aluminium wall in contact with the cooling/heating fluid
Re	[-]	Reynolds number
S_e	[W/m^3]	Volumetric rate of heat generation
$\vec{S}_m$	[N/m^3]	Volumetric momentum source term
T	[K]	Temperature
$T_{ch,m}$	[K]	Mean temperature of the heating/cooling fluid in the channel
$T_{ch,i}$	[K]	Temperature of the heating/cooling fluid at the inlet section of the channel
$T_{ch,o}$	[K]	Temperature of the heating/cooling fluid at the outlet section of the channel
T_i	[K]	Initial temperature
T_0	[K]	Temperature of the PCM
$T_{sl,1}$	[K]	Higher phase change temperature of the PCM
$T_{sl,2}$	[K]	Lower phase change temperature of the PCM
$T_{w,1}$	[K]	Temperature of the aluminium wall-surface in contact with the PCM
$T_{w,2}$	[K]	Temperature of the aluminium wall-surface in contact with the cooling/heating fluid
t	[s]	Time
V	[m^3]	Volume of the cell
u	[m/s]	Velocity in x-direction
$\vec{v}$	[m/s]	Velocity vector
$\vec{v}_p$	[m/s]	Drag velocity vector of the solid phase
x	[m]	Coordinate axis in the direction of the aluminium plate thickness

Special characters

β	[-]	Volumetric fraction of the PCM liquid phase
ε	[-]	Constant in equation (2)
θ	[-]	Dimensionless parameter of temperature
μ	[kg/m s]	Dynamic viscosity
μ_0	[kg/m s]	Dynamic viscosity evaluated at $T_{w,2}$
ρ	[kg/m^3]	Density

Subscripts

E	Centre of the East adjacent control volume
m	Melting
P	Centre of the control volume
s	Solidification
W	Centre of the West adjacent control volume

Superscripts

0	Previous time step

NUMERICAL STUDY

A physical model of the system is presented below in detail. Then, the computational procedure is discussed.

Physical Model

A schematic view of the two-dimensional computational domain is shown in Figure 1, where three regions, rectangular PCM, parallel flat plates of aluminium containing the PCM and channels for the heating/cooling fluid, can be appreciated. Figure 1(a) shows the horizontal arrangement and Figure 1(b) shows the vertical arrangement.

The figure also presents the nomenclature for the variables: $T_{w,1}$ is the temperature of the aluminium wall at the surface in contact with the PCM, $T_{w,2}$ is the temperature of the aluminium wall at the surface in contact with the heating/cooling fluid, T_0 is the temperature of the PCM representing the temperature in the entire PCM sub-domain, $T_{ch,i}$ is the temperature of the heating/cooling fluid at the inlet section of the channel, and $\dot{m}_{ch}$ is the mass flow rate of the heating/cooling fluid, for which half the flow through the channel is considered due to the symmetry of the problem.

The boundary conditions when solving the CFD numerical model in the complete set "PCM module-water channels" (boundary condition of the third kind) are: mass flow rate of the cooling/heating fluid at the inlet of the channels, pressure of the heating/cooling fluid at the outlet of the channels, symmetry at the central planes of the channels (top and bottom borders of the domain in the horizontal arrangement, right and left borders of the domain in the vertical arrangement) because only half the width of the channels is considered and null heat flux at the ends (right and left sides in the horizontal arrangement, top and bottom sides in the vertical arrangement) of the PCM module.

The geometric dimensions are: module length of L=0.2 m, PCM thickness e_{PCM}=30 mm, aluminium thickness of 0.015 m and water channel width of e_{ch}=0.004 m.

The properties of the aluminium are: density 2719 kg/m^3, specific heat 871 J/kg K and thermal conductivity 202.4 W/m K. The thermal properties of the water are taken from the data in [11], and were accurately fitted by polynomial expressions. The density and the viscosity of the PCM are presented in Table 1. The specific heat of the PCM is 6067 J/kg K for the solid phase and 2340 J/kg K for the liquid phase. The solid-

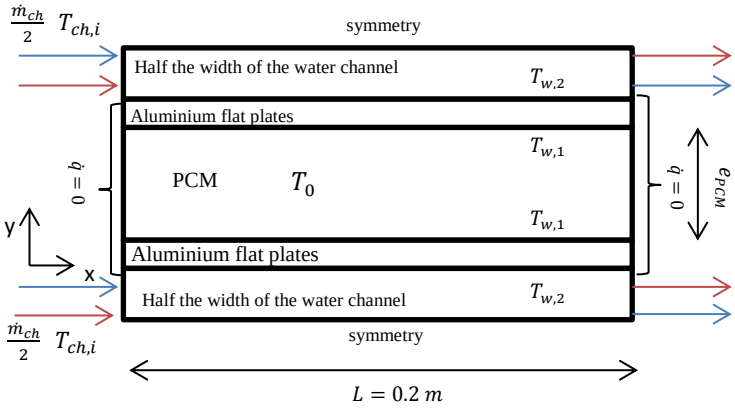

(a) Horizontal arrangement

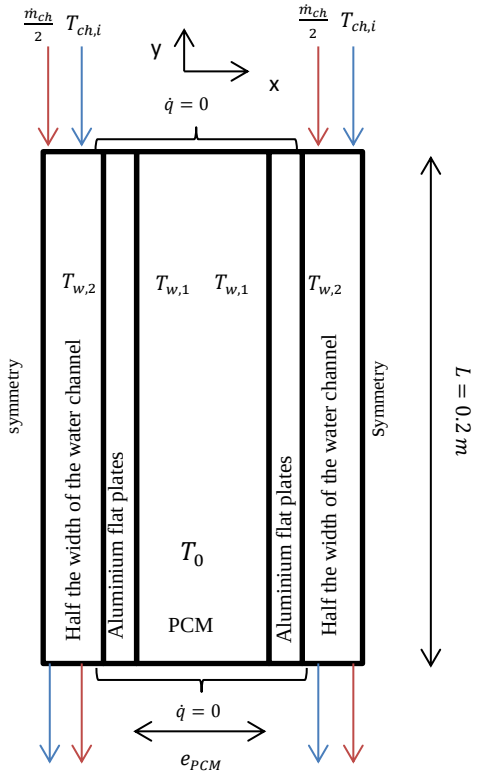

(b) Vertical arrangement

Figure 1 Computational domains

Table 1 Properties of the PCM

T (K)	ρ (kg/m^3)	μ (kg/m s)
326	880.00	10.0
334	770.00	0.02853
335	769.23	0.02850
338	766.92	0.02841
341	764.61	0.02833
344	762.30	0.02824
347	759.99	0.02816
350	757.68	0.02807
353	755.37	0.02799
363	747.67	0.02770

liquid phase change latent heat of the PCM is 100892 J/kg. The thermal conductivity of the PCM is considered constant and equal to 0.2 W/m K

Computational grid

The computational domain is divided into a grid of rectangular cells to solve the full CFD model. The number of cells for the three sub-domains (or regions) in the horizontal and vertical arrangements is shown in Table 2.

Table 2 Computational grid (CFD model)

	Horizontal arrangement		Vertical arrangement		
Sub-domain	**x**	**y**	**x**	**y**	**Total number of cells**
PCM	100	30	30	100	3000
Aluminium flat plates	100	6	6	100	600
Half the width of the water channel	100	8	8	100	800

In the fast numerical model, the phase change within the PCM sub-domain is solved applying the CFD numerical model to the two-dimensional grid indicated in Table 2 for the PCM sub-domain. Besides, boundary conditions of null heat flux at the ends (right and left sides in the horizontal arrangement, top and bottom sides in the vertical arrangement) and prescribed temperature (boundary condition of the first kind) at the borders of length *L* (top and bottom sides in the horizontal arrangement, right and left sides in the vertical arrangement) are considered. In each aluminium flat plate sub-domain, the model is solved using a one-dimensional grid of eight cells along the thickness of the plate. Each cell is *L* in length and its thickness is equal to the thickness of the plate divided by eight. Finally, in each water channel sub-domain, the model is solved using a one-dimensional grid of twenty cells along the length of the channel. Each cell is e_{ch} in width and its length is equal to the length of the channel divided by twenty.

Equations

(a) PCM sub-domain

The behavior of the PCM during the phase change (melting and solidification) is simulated using a model implemented in the software Ansys Fluent 14.5. The model uses an enthalpy-porosity formulation [12]. The liquid fraction, β, is defined as the fraction of the cell volume that is in liquid form. In the model, the liquid-solid mushy zone is treated as a porous zone with porosity equal to the liquid fraction. The porosity lies between 0 and 1, according to the progress of the melting or solidification process.

The energy balance is given by equation (1):

$$\frac{\partial}{\partial t}(\rho i) + \nabla \cdot (\rho \vec{v} i) = \nabla \cdot (k \nabla T) + S_e \qquad (1)$$

where ρ is the density, i the enthalpy, $\vec{v}$ the velocity, k the thermal conductivity, T the temperature and S_e the volumetric rate of heat generation. The solution of the problem is essentially an iterative process between the energy equation and the liquid fraction equation, indicated in equation (2):

$$\beta = \frac{T - T_{sl2}}{T_{sl1} - T_{sl2}} \quad (2)$$

Regarding the momentum equation (3), the momentum source term expressed by equation (4), $\vec{S}_m$, is added due to the reduced porosity in the mushy zone:

$$\frac{\partial}{\partial t}(\rho\vec{v}) + \nabla\cdot(\rho\vec{v}\vec{v}) = -\nabla\rho + \nabla\cdot(\bar{\bar{\tau}}) + \rho\vec{g} + \vec{S}_m \quad (3)$$

$$\vec{S}_m = \frac{(1-\beta)^2}{(\beta+\epsilon)} A_{mush}\left(\vec{v} - \overrightarrow{v_p}\right) \quad (4)$$

where ε is a small number (0.001) to prevent division by zero, A_{mush} is the mushy zone constant (100000 kg/s m^3) that measures the amplitude of the damping; the higher this value, the steeper the transition of the velocity of the material to zero as it solidifies, and $\overrightarrow{v_p}$ accounts for the movement of the solidified material out of the domain, so in this case it is equal to 0.

(b**) Aluminium flat plates and water channels sub-domains**

Figure 2 shows the finite volumes and the nomenclature used in the modeling of the aluminium flat plates and the water channels.

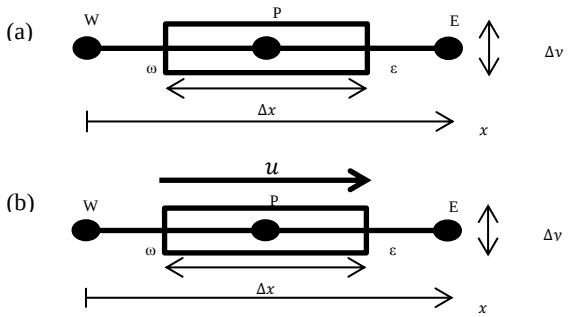

Figure 2 Nomenclature for the finite volumes: (a) aluminium flat plates, (b) water channels

The energy equation in the aluminium flat plate region is solved using an unsteady fully-implicit scheme [13]. The spatial diffusion effects (right side of the energy equation) are solved applying a central differencing approximation, considering linear interpolation between the values of the temperature at the centre of the neighbour finite volumes. Equation (5) expresses the energy equation in an inner node:

$$\frac{\rho c_p\left(T_P - T_P^0\right)}{\Delta t}\Delta x = \frac{k}{\Delta x}\left(T_E - T_P\right) - \frac{k}{\Delta x}\left(T_P - T_W\right) \quad (5)$$

where x is the coordinate axis along the thickness of the plate, subscript P is the centre point of the calculation finite volume, subscripts W and E are the centre points of the neighbour finite volumes and superscript 0 refers to the previous time step.

In the boundary nodes, equation (6) is applied to the finite volume in contact with the heating/cooling fluid channel, whereas equation (7) is applied to the finite volume in contact with the PCM, where the heat flux through the aluminium plate wall-surface in contact with the PCM fluid is $\dot{q}_{w,1}$.

$$\frac{\rho c_p\left(T_P - T_P^0\right)}{\Delta t}\Delta x = \frac{2k}{\Delta x}\left(T_{w,2} - T_P\right) - \frac{k}{\Delta x}\left(T_P - T_W\right) \quad (6)$$

$$\frac{\rho c_p\left(T_P - T_P^0\right)}{\Delta t}\Delta x = \frac{k}{\Delta x}\left(T_E - T_P\right) - \dot{q}_{w,1} \quad (7)$$

The energy equation in the cooling/heating fluid channel region is solved using also an unsteady fully-implicit scheme [13]. In this case, the spatial diffusion and convection effects (right and left side of the equation, respectively) are solved applying an upwind differencing scheme that takes into account the flow direction when determining the values of the temperature at the finite volume faces. Equation (8) expresses the energy balance in an inner node, whereas equations (9) and (10) represent respectively the energy balance in the boundary nodes corresponding to the inlet and the outlet of the channel. In these equations, (8)-(10), x is the coordinate axis along the length of the channel, L, and the effect of the PCM is introduced by means of the heat flux through the aluminium plate wall-surface in contact with the heating/cooling fluid, $\dot{q}_{w,2}$. The temperature at the inlet of the channel, $T_{ch,i}$, appears in equation (9), whereas the temperature at the outlet of the channel, $T_{ch,o}$, is identified in equation (10) to the calculated temperature, T_P, because of the upwind scheme.

$$\rho c_p\left(T_P - T_P^0\right)\frac{\Delta x}{\Delta t} + \rho c_p u\left(T_P - T_W\right) = \frac{k}{\Delta x}\left(T_E - T_P\right) - \frac{k}{\Delta x}\left(T_P - T_W\right) + 2\dot{q}_{w,2}\frac{\Delta x}{e_{ch}} \quad (8)$$

$$\rho c_p\left(T_P - T_P^0\right)\frac{\Delta x}{\Delta t} + \rho c_p u\left(T_P - T_{ch,i}\right) = \frac{k}{\Delta x}\left(T_E - T_P\right) - \frac{k}{\Delta x}\left(T_P - T_{ch,i}\right) + 2\dot{q}_{w,2}\frac{\Delta x}{e_{ch}} \quad (9)$$

$$\rho c_p\left(T_P - T_P^0\right)\frac{\Delta x}{\Delta t} + \rho c_p u\left(T_P - T_W\right) = \frac{k}{\Delta x}\left(T_P - T_W\right) + 2\dot{q}_{w,2}\frac{\Delta x}{e_{ch}} \quad (10)$$

(c) Interphase "aluminium flat plate-PCM"

The condition of continuity at the interphase "aluminium flat plate-PCM" is expressed in equation (11). Likewise, equation (12) shows the continuity condition at the interphase "aluminium flat plate-heating/cooling fluid", where $T_{ch,m}$ is the mean temperature of the heating/cooling fluid in the channel. The convective heat transfer coefficient, h, is evaluated from a correlation obtained for this case in particular, equation (13), since the available correlations in the literature did not give good results for the geometry and length of the channel and the mass flow rate conditions through it.

$$\frac{2k}{\Delta x}\left(T_P - T_{w,1}\right) = \dot{q}_{w,1} \quad (11)$$

$$\frac{2k}{\Delta x}\left(T_P - T_{w,2}\right) = h\left(T_{w,2} - T_{ch,m}\right) \quad (12)$$

$$\mathrm{Nu} = 1.65\ \mathrm{Re}^{0.232}\ \mathrm{Pr}^{0.223}\left(\frac{\mu}{\mu_0}\right)^{0.0173} \quad (13)$$

$$100 < \mathrm{Re} < 1000$$

$$2.4 < \mathrm{Pr} < 5$$

$$0.7 < \frac{\mu}{\mu_0} < 1.3$$

$$h = \frac{\mathrm{Nu}\ k}{L_c} \quad (14)$$

The characteristic length in the dimensionless numbers is $L_c = 2e_{ch} = 8\ mm$.

All the properties in the correlation are evaluated at the mean temperature of the heating/cooling fluid, except μ_0, that is

evaluated at the temperature of the aluminium wall-surface in contact with the heating/cooling fluid.

Application of the boundary conditions

Figure 3 shows the temperature evolution of the paraffin RT60 as it cools from the liquid state. The solidification process starts at the high phase change temperature T_{sl1}=334 K and finishes at the low phase change temperature T_{sl2}=326 K.

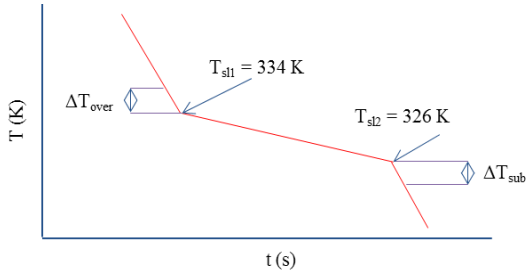

Figure 3 Temperature evolution of the paraffin during solidification

The boundary conditions applied to the first kind problem (known temperature at the borders of the PCM module in contact with the heating/cooling fluid) are given in Table 3. The values of a dimensionless parameter of temperature, θ, which is used in the discussion of the results, are also included.

Table 3 Boundary conditions in the first kind problem

θ	$T_{w,1}$ (K)	
	Melting	**Solidification**
θ1=0.82	335	325
θ2=0.90	344	315
θ3=0.95	361	298

The dimensionless parameter of temperature is defined in equations (15) and (16) for the melting and solidification processes, respectively:

$$\theta_m = \frac{T_{w,1}-T_{sl2}}{T_{w,1}-T_i} \quad \Delta T_{sub} = T_{sl2} - T_i \qquad (15)$$

$$\theta_s = \frac{T_{sl1}-T_{w,1}}{T_i-T_{w,1}} \quad \Delta T_{over} = T_i - T_{sl1} \qquad (16)$$

A 2K subcooling and superheating of the paraffin with respect to the high and low phase change temperatures are considered. The subcooling and the superheating define the initial condition of temperature, T_i, which is 324 K for the melting and 336 K for the solidification.

The boundary conditions applied to solve the third kind problem, mass flow rate and temperature of the heating/cooling fluid at the inlet of the channel, are: 0.1 kg/s and 348 K for the melting in both arrangements, vertical and horizontal, 0.2 kg/s and 313 K for the solidification in the vertical arrangement, and 0.1 kg/s and 313 K for the solidification in the horizontal arrangement.

Calculation procedure

Figure 4 presents the calculation procedure. At a given time step, the temperature fields associated to the previous time step are known: T^o_{w1},. T^o_{w2}, $T^o_{ch,o}$.With the last temperaure value the mean temperature $T^o_{ch,m}$ is calculated and asignated as a first value for $T_{ch,m}$. The "subroutine interphase" includes, besides the interphase equations, the calculation of the temperatures of the aluminium flat plates sub-domains and particularly $T_{w,1}$, $T_{w,2}$and also the calculation of the heat flux at the flat plate surfaces in contact with the PCM and in contact with the heating/cooling fluid, $\dot{q}_{w,1}$, $\dot{q}_{w,2}$, respectively. Inside this subroutine, the initial values of the temperatures at the interphases are equal to the ones obtained in the previous time step, $T^o_{w,1}$,. T^o_{w2}. Then these values are calculated and checked according to the energy balance equations until convergence. As stated before, the value of the heat flux transmitted to the water, $\dot{q}_{w,2}$, is obtained from that subroutine.. Subsequently, the subroutine "Water channel" starts taking the last heat flux. This subroutine produces a new value for the mean temperature of the water at the outlet of the channel $T_{ch,m,new}$. This value is checked against $T_{ch,m}$ and if the values are more different than a quantity, the value of the mean temperature at the outlet of the channel is reasignated to $T_{ch,m,new}$. This value then enters one more time the subroutine "interphase" until it fullfills the convergence criteria indicated in Table 4.

All the equations and the iterative calculation procedure are implemented in a Matlab R2012a.

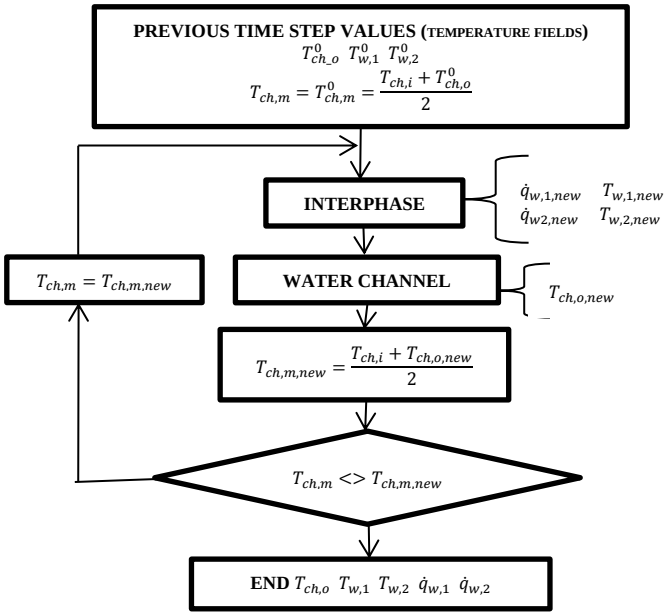

Figure 4 Flow chart showing the calculation procedure in a time step

Table 4 Convergence criteria

Variable	Calculation subroutines affected	criteria	value
$\dot{q}_{w1}$	INTERPHASE	Relative differences in the balance of equation	2%
$\dot{q}_{w2}$	INTERPHASE	Relative differences in the balance of equation	2%
$T_{ch,m}$	WATER CHANNEL AND INTERPHASE	Absolute differences of the media temperatures between consecutive iterations	10^{-4} K

RESULTS AND DISCUSSION

Phase change sub-domain

Figure 5 presents the velocity field for θ=0.9 and both phase change processes, melting and solidification, in case of horizontal position of the PCM for a given instant of time. A cellular flow is observed in different positions within the PCM depending on the process. For the melting, the cellular flow is close to the bottom: the liquid is lighter than the solid and moves up, thus producing free convection. Nevertheless, the extension of the liquid movement is limited by the presence of the PCM above that is still solid. However, the liquid that would be produced at the top would not be able to go any higher because of the boundary. As for the solidification process, the cellular flow is close to the top: the solidification starts at the boundaries and is fast enough to promote the progress from the sides to the centre, so that nearly a symmetrical behaviour can be observed. Anyway, the PCM that is still liquid tends to be closer to the upper part because of the lower density of the liquid. This flow produces asymmetry in the velocity field, and consequently, also in the temperature field.

Figure 6 presents the velocity field for θ=0.9 and both phase change processes, melting and solidification, in case of vertical position of the PCM for a given instant of time. Symmetry is observed in the entire domain. This flow produces lower heat transfer rate than in the horizontal position of the PCM and also symmetry in the temperature field. For the melting, greater velocities are observed near the walls of the module because the liquid has lower density than the solid and moves up. For the solidification, the heat transfer rate at the boundaries is much faster, which causes the solidification to move from the sides to the centre. Besides, the PCM that is still liquid, moves up to reach the top and two symmetrical vortexes appear when most of the PCM is already solid.

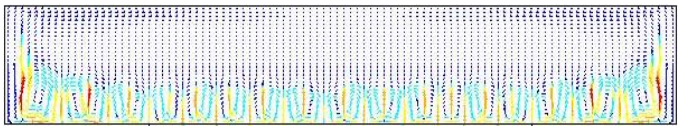

(a) Melting (60% liquid)

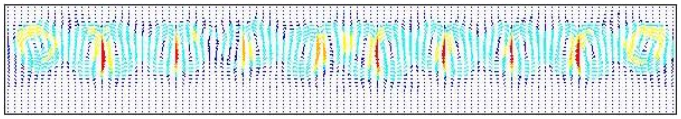

(b) Solidification (60% solid)

Figure 5 Velocity fields for the horizontal position of the PCM

The boundary conditions presented in Table 3 are applied to the PCM and results of the liquid fraction, β, and the heat flux, $\dot{q}$, are obtained throughout time for different values of the dimensionless parameter of temperature, θ. As an example of these results, Figure 7(a) presents the variation of the liquid fraction during the melting process within the PCM in vertical position, for the three values of the parameter θ. A great influence of θ on the time of the process can be observed: as the value of the parameter decreases from θ_3=0.95 (for the highest temperature at the boundary $T_{w,1}$=361 K) to θ_1=0.82 (for the lowest temperature at the boundary $T_{w,1}$=335 K), the duration of the process increases from less than 2000 seconds to more than 7000 seconds.

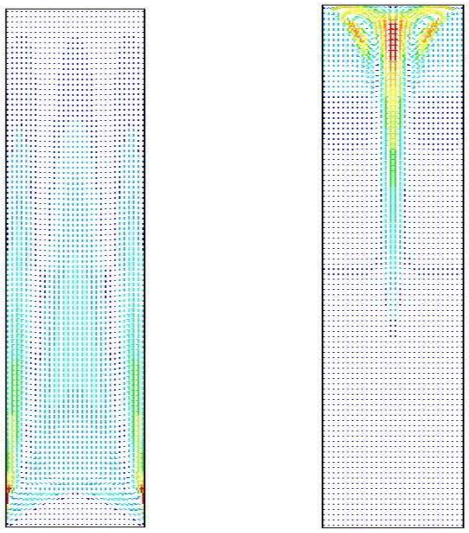

(a) Melting (95% liquid), (b) solidification (95% solid)

Figure 6 Velocity fields for the vertical position of the PCM

Figure 7(b) presents the variation of the heat flux along the melting process within the PCM in vertical position, for the three values of the parameter θ. As this parameter decreases from θ_3 to θ_1, the heat flux diminishes very much. In particular, the fastest rates, which are produced at the beginning of the process, change from 15000 W/m^2 to 5000 W/m^2.

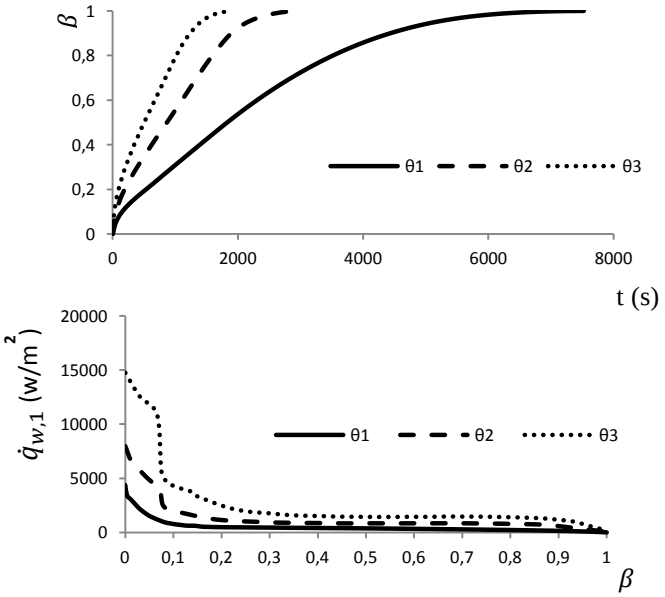

Figure 7 Melting process for the vertical position of the PCM: (a) function $\beta(t)$, (b) function of the heat flux at the interface aluminium-water. First kind boundary condition.

In the same way, results for the melting process within the PCM in horizontal position and also results for melting and solidification processes within the PCM in vertical and horizontal position, are obtained. Subsequently, these results are correlated into mathematical equations of the type shown in equations (17) and (18). Firstly, a combination of polynomials and exponential functions expresses the liquid fraction, β, depending on the phase change mechanism (melting or solidification), the spatial position of the PCM (horizontal or vertical), the dimensionless parameter of temperature, θ, and the time. Secondly, a combination of polynomial functions expresses the heat flux from the PCM, $\dot{q}_{w,1}$, depending on the phase change mechanism, the spatial position of the PCM and the liquid fraction.

$$\beta = \beta(mechanism, position, \theta, t) \quad (17)$$

$$\dot{q}_{w,1} = \dot{q}_{w,1}(mechanism, position, \beta) \quad (18)$$

This procedure leads to a better approximation of the values obtained using the CFD model. The combination of equations (17) and (18) gives expressions of the type indicated in equation (19):

$$\dot{q}_{w,1} = \dot{q}_{w,1}(mechanism, position, \theta, t) \quad (19)$$

Figure 8 presents the variation of the heat flux versus time for melting (upper part of the graph) and solidification processes (lower part of the graph) within the PCM in vertical position and for the three values of θ. It can be appreciated that the solidification process is longer that the corresponding melting process and also that the heat fluxes are consequently lower in solidification than in melting.

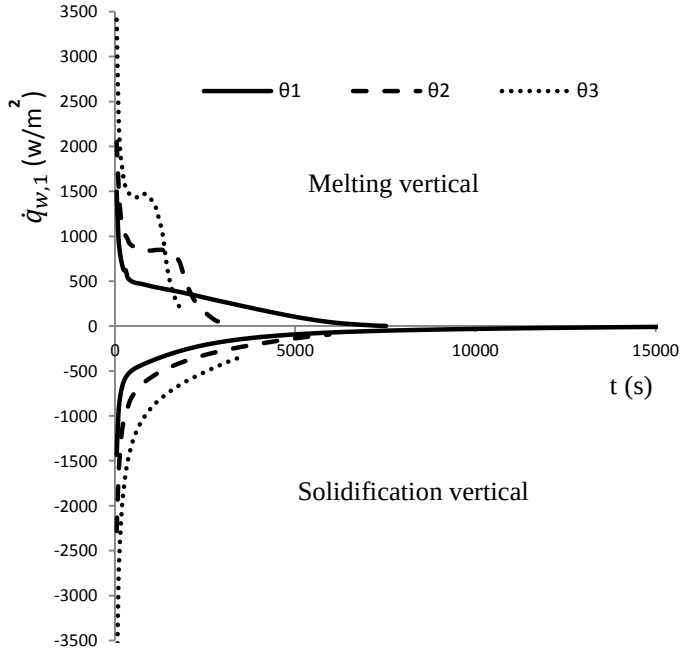

Figure 8. Heat flux at the interface aluminium-water for the melting and solidification processes within the PCM in vertical position.

Figure 9 presents the variation of the heat flux versus time for melting (upper part of the graph) and solidification processes (lower part of the graph) within the PCM in horizontal position and for the three values of θ. As in Figure 8, it can be appreciated that the solidification process is longer that the corresponding melting process and also that the heat fluxes are consequently lower in solidification than in melting. Regarding the PCM in vertical position, the length of the processes is diminished for the three values of θ, but it is appreciated more clearly for θ_1 (the slowest heat flux).

To sum up the observations in both figures 8 and 9 and with reference to θ_1 (the slowest heat flux), for the solidification process the vertical position happens to give a timing of 16617 seconds while the horizontal position gives a duration of 13609 seconds. In the same way, for the melting process the vertical position gives a timing of 7525 seconds while the horizontal position gives duration of 4551 seconds.

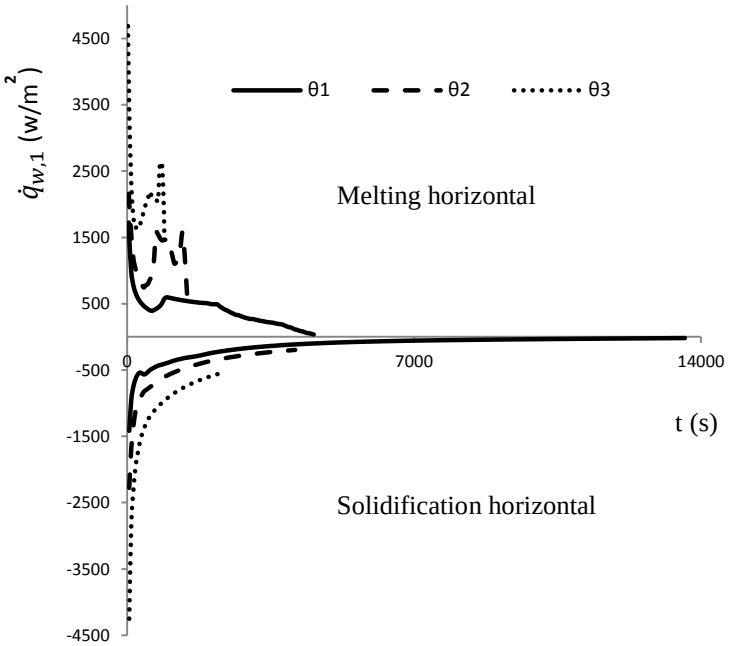

Figure 9 Heat flux at the interface aluminium-water for the melting and solidification processes within the PCM in horizontal position.

Comparison of the fast model

The fast model couples the equations (17)-(18) obtained for the PCM sub-domain, with the finite volume equations applied to the solid (aluminium flat plates) and water (heating/cooling fluid) sub-domains. The results of the fast model are now compared with the results of the full CFD model, which couples simultaneously the three sub-domains and solves the problem in Ansys Fluent 14.5 The comparison is based on the heat flux at the interphase "aluminium flat plate-water", $\dot{q}_{w,2}$, and the temperature of the water at the outlet of the channel, $T_{ch,o}$.

In Figures 10 and 11, the results for both processes, the melting and the solidification, in case of the vertical position of the module are compared. Figure 10 shows the heat flux at the

interphase "aluminium flat plate-water" and Figure 11 shows the temperature of the water at the outlet of the channel. The solid line represents the results of the full CFD model, whereas the dash line represents the results of the fast model. The figures also include the values of the boundary conditions applied to the water in the full CFD model. A good approach of both models can be appreciated.

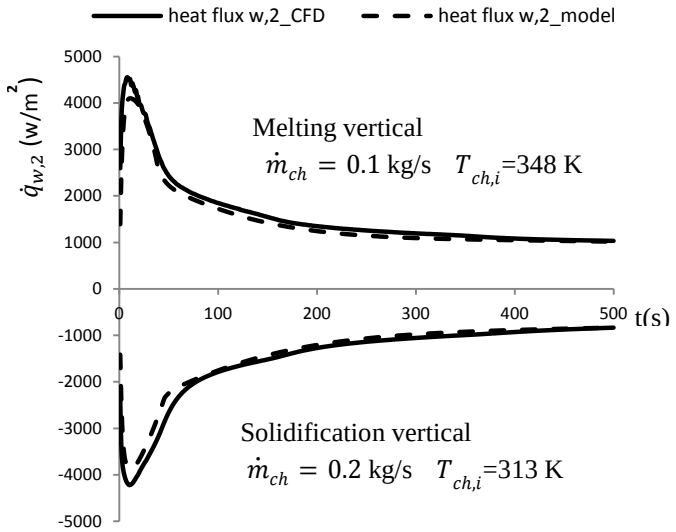

Figure 10 Comparison of CFD and fast model results of the heat flux at the interphase "aluminium flat plate-water" for the vertical position of the module.

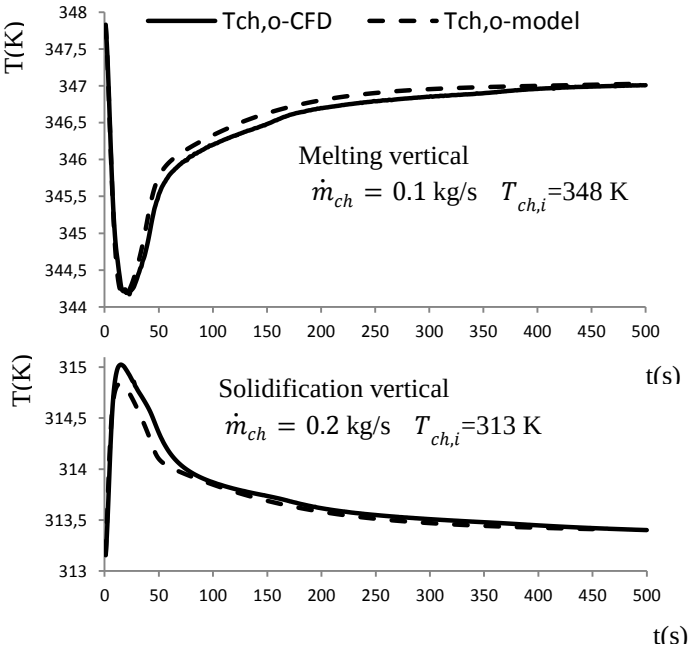

Figure 11 Comparison of CFD and fast model results of the water temperature at the outlet of the channel for the vertical position of the module.

In Figures 12 and 13, the results for both processes, melting and solidification, in case of the horizontal position of the module are compared. Figure 12 shows the heat flux at the interphase "aluminium flat plate-water" and Figure 13 shows the temperature of the water at the outlet of the channel. The boundary conditions applied to the water in the full CFD model are the same as in the case of the vertical position. Similar results can be appreciated for both models, although the values of the melting process differ more as the time passes by. Figure 14 completes until practically the end of the process (85% melted) the values in Figure 12, showing that the models do not diverge after the time elapsed represented in Figure 12 for the melting horizontal case.

The variables presented in figures (7)-(13) are obtained from the CFD model by averaging the values in the cell surfaces or in the cell volumes according to equations (20)-(24).

- Liquid fraction:

$$\beta = \frac{1}{V}\int_V \beta dV = \frac{1}{V}\sum_{i=1}^{n} \beta_i |V_i| \quad (20)$$

- Mean bulk temperature:

$$T_0 = \frac{\int_V \rho T dV}{\int_V T dV} = \frac{\sum_{i=1}^{n} \rho_i T_i |V_i|}{\sum_{i=1}^{n} \rho_i |V_i|} \quad (21)$$

- Wall heat fluxes, $\dot{q}_{w,1}$ and $\dot{q}_{w,2}$:

$$\dot{q}_w = \frac{1}{A}\int_A \dot{q} dA = \frac{1}{A}\sum_{i=1}^{n} \dot{q}_i |A_i| \quad (22)$$

- Wall temperatures, $T_{w,1}$ and $T_{w,2}$:

$$T_w = \frac{1}{A}\int_A T dA = \frac{1}{A}\sum_{i=1}^{n} T_i |A_i| \quad (23)$$

- Temperature at the outlet of the channel:

$$T_{ch,o} = \frac{\int_A \rho T |\vec{v}\cdot\vec{dA}|}{\int_A \rho |\vec{v}\cdot\vec{dA}|} = \frac{\sum_{i=1}^{n} \rho_i T_i |\vec{v}_i\cdot\vec{A}_i|}{\sum_{i=1}^{n} \rho_i |\vec{v}_i\cdot\vec{A}_i|} \quad (24)$$

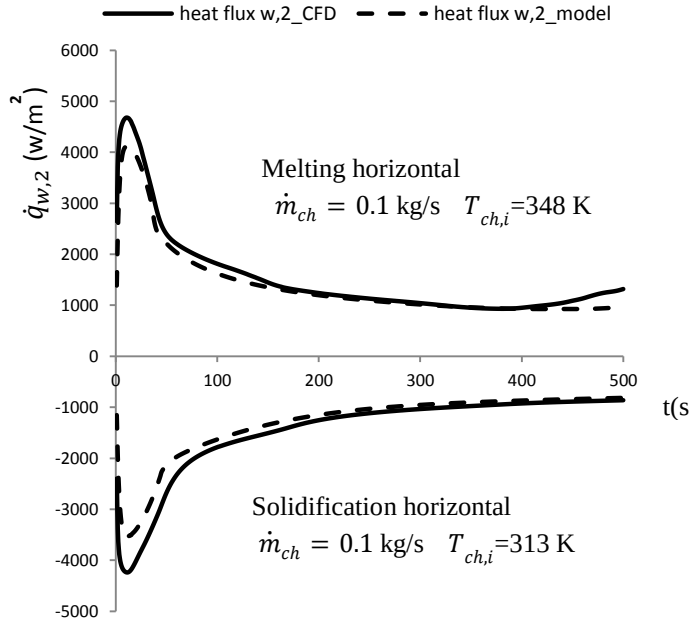

Figure 12 Comparison of CFD and fast model results of the heat flux at the interphase "aluminium flat plate-water" for the horizontal position of the module.

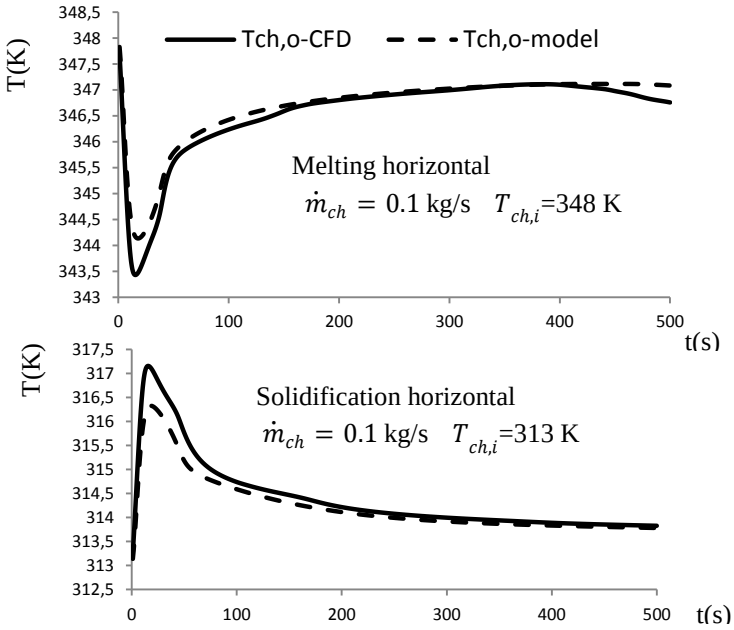

Figure 13 Comparison of CFD and fast model results of the water temperature at the outlet of the channel for the horizontal position of the module

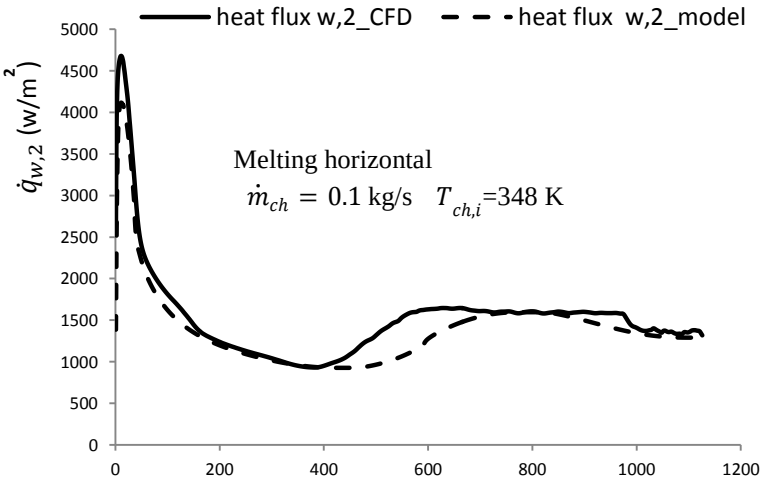

Figure 14 Comparison of CFD and fast model results of the heat flux at the interphase "aluminium flat plate-water" for the horizontal position of the module (85% of the melting process, 1130 seconds)

Table 5 summarizes the average absolute and relative differences between the models considering all the instants of time represented in the figures for both processes (solidification and melting) and for both spatial positions of the module (vertical and horizontal).

Average absolute errors are used for the temperatures, whereas average relative errors are used for the liquid fraction and the heat fluxes.

Table 5 Average errors: Validation 500s

	Solidification vertical	**Melting vertical**	**Solidification horizontal**	**Melting horizontal**
Inlet	$\dot{m}_{ch}$ = 0.2 kg/s $T_{ch,i}$=313 K	$\dot{m}_{ch}$ = 0.1 kg/s $T_{ch,i}$=348 K	$\dot{m}_{ch}$ = 0.1 kg/s $T_{ch,i}$=313 K	$\dot{m}_{ch}$ = 0.1 kg/s $T_{ch,i}$=348 K
Average absolute errors (K) $\varepsilon_a = \frac{\sum_1^n \lvert T_{CFD} - T_{model} \rvert}{n}$				
T_{ch_o}	0.051	0.100	0.161	0.127
$T_{w,1}$	0.075	0.234	0.549	0.598
$T_{w,2}$	0.074	0.079	0.552	0.600
T_0	0.363	0.306	0.108	0.215
Average relative errors $\varepsilon_r = \frac{1}{n}\sum_1^n \left\lvert \frac{value_{CFD} - value_{model}}{value_{CFD}} \right\rvert$				
β	0.046	0.255	0.028	0.182
$\dot{q}_{w,1}$	0.064	0.079	0.099	0.083
$\dot{q}_{w,2}$	0.057	0.065	0.092	0.074

The approach between the models is always better for the vertical than for the horizontal position due to the unsteady cellular flow. The errors in vertical position are lower for solidification than for melting, except for T_0 in vertical melting, in which the errors are very close. However, the errors in horizontal position are quite similar in solidification and in melting. Even though there are some situations in which greater errors in temperature are found (nearly to 0.6 K), they do not imply important relative heat flux errors.

The computational requirements for a CFD simulation are extremely high. The net computational time depends on the boundary conditions, but in general, a simulation takes several weeks in a computer with 8 cores Opteron 2356, 2.3 GHz/core. Conversely, the fast model takes few hours to obtain a solution. Therefore, in view of the errors mentioned above, it might be concluded that the fast model will facilitate the design and study of domestic heat exchangers containing quite a lot modules in a domain of 0.8×0.6×0.6 m^3.

CONCLUSIONS

The heat transfer during the solid-liquid phase change of the paraffin RT60 has been studied in rectangular modules of the PCM covered with aluminium and cooled by water. A fast numerical model has been developed which includes the results obtained from the CFD phase change simulation through handy equations. These equations have been implemented in a Matlab program along with a finite volume set of equations to solve the

heat transfer in the aluminium covering and the water that heats/cools the PCM.

The results of the fast model have been satisfactorily compared with the results of the full CFD model that couples the heat transfer within the three regions: PCM, aluminium covering and heating/cooling water. The computational time is reduced to few days in the fast model with respect to the requirements of the full CFD model, which is about several weeks.

A specific correlation has been obtained to calculate the heat transfer convection coefficient in channels that would be present in heat exchangers with PCM modules similar to the one proposed in this work. The correlations available in the literature were not adequate for this process.

The processes of melting and solidification of PCM modules in vertical and horizontal spatial position have been analysed. The solidification in the vertical position is slower than in the horizontal position. The melting process is also slower in the vertical position, the melting time in the horizontal position being nearly twice the melting time in the vertical position.

ACKNOWLEDGEMENTS

We wish to express our gratitude to the Spanish Program of Research and Development (Plan Nacional de Investigación) for its financial support under project SV-PA-13-ECOEMP-24, which made this research work possible.

REFERENCES

[1] Hassana M.M., Beliveau Y., Modeling of an integrated solar system, *Building and enviroment*, Vol. 43, 2008, pp. 804-810

[2] Nagano K., Takeda S., Mochida T., Shimakura K., Nakamura T., Study of a floor supply air conditioning system using granular phase change material to augment building mass thermal storage-Heat response in small scale experiments.*Energy and buildings*, vol. 38, 2006 , pp. 436-446

[3] Anica Trp., An experimental numerical investigation of heat transfer during technical grade paraffin melting and solidification in a shell-and-tube latent thermal energy storage unit , *Solar Energy*, Vol. 79, , 2005, pp. 648-660

[4] Mosaffa A.H., Talati F., Rosen M.A., Basirat Tabrizi H., Aproximate analytical model for PCM solidification in a rectangular finned container with convective cooling boundaries, *International communications in Heat and Mass Transfer*, Vol. 39, 2012, pp. 318-324

[5] Felix Regin A., Solonki S.C., Saini J.S., An analysis of a packed bed latent heat thermal energy storage system using PCM capsules:Numerical investigation, *Renewable Energy*, Vol. 34, 2009, pp. 1765-1773

[6] Dolado P., Lazaro A., Martin J.M., Zalba B., Characterization of melting and solidification in a real scale PCM-air heat exchanger:Numerical and experimental validation, *Energy Conversion and Management*, Vol. 52, 2011, pp. 1890-1907

[7] Rostamizadeh M., Khanlarkhani M., Sadrameli M., Simulation energy storage system with phase change material(PCM), *Energy and Buildings*, Vol. 49, 2012, pp. 419-422

[8] Belusko M., Halowa E., Bruno F., Characterising PCM thermal storage systems using the effectiveness-NTU approach, *International Journal of Heat and Mass Transfer*, Vol. 52, 2012, pp. 3359-3365

[9] RUBITHERM® RT http://www.rubitherm.de/english/pages/02a_latent_heat_pcms.htm

[10] ANSYS FLUENT 14.5 Theory Guide

[11] Mills A.F., Heat and MassTransfer, *Burr Ridge, Illinois, U.S.A.: Richard Irwin*, 1995

[12] Voller V.R., Swaminathan C.R., Generalize Source-based Method for solidification phase change, *Numer. Heat and Transfer B*, Vol.19(2), 1991, pp.175-189

[13] Versteg H.K., Malalasekera W., An introduction to Computational Fluid Dynamics: The finite volume method, *Longman Scientific & Technical*, First edition 1995